Selective CO_2 Capture in ZIFs | Hot Paper

DOI: 10.1002/ange.201403980

Selective Capture of Carbon Dioxide under Humid Conditions by Hydrophobic Chabazite-Type Zeolitic Imidazolate Frameworks**

*Nhung T. T. Nguyen, Hiroyasu Furukawa, Felipe Gándara, Hoang T. Nguyen, Kyle E. Cordova, and Omar M. Yaghi**

Abstract: *Hydrophobic zeolitic imidazolate frameworks (ZIFs) with the chabazite (**CHA**) topology are synthesized by incorporating two distinct imidazolate links. $Zn(2\text{-mIm})_{0.86}(bbIm)_{1.14}$ (ZIF-300), $Zn(2\text{-mIm})_{0.94}(cbIm)_{1.06}$ (ZIF-301), and $Zn(2\text{-mIm})_{0.67}(mbIm)_{1.33}$ (ZIF-302), where 2-mIm = 2-methylimidazolate, bbIm = 5(6)-bromobenzimidazolate, cbIm = 5(6)-chlorobenzimidazolate, and mbIm = 5(6)-methylbenzimidazolate, were prepared by reacting zinc nitrate tetrahydrate and 2-mIm with the respective bIm link in a mixture of N,N-dimethylformamide (DMF) and water. Their structures were determined by single-crystal X-ray diffraction and their permanent porosity shown. All of these structures are hydrophobic as confirmed by water adsorption isotherms. All three ZIFs are equally effective at the dynamic separation of CO_2 from N_2 under both dry and humid conditions without any loss of performance over three cycles and can be regenerated simply by using a N_2 flow at ambient temperature.*

Zeolitic imidazolate frameworks (ZIFs) are a class of porous, crystalline materials, in which metal atoms are connected through ditopic imidazolate ($C_3N_2H_3^- = Im$) or functionalized Im bridges.[1] The resulting open frameworks exhibit topologies that are analogous to those observed in microporous zeolites. Although there has been over one hundred ZIF structures reported, few of these have topologies found for the most important zeolites.[2] Two strategies have been utilized to overcome this challenge and make topologies known to be important in zeolite chemistry. In the first, link–link interactions are used to direct the synthesis to a specific topology as was demonstrated for ZIF-20 having the common **LTA** zeolite topology.[3,4] In the second strategy, mixed links are used to produce ZIF-68 to ZIF-70 and ZIF-78 to ZIF-82, which are based on the **GME** zeolite topology.[4–6] Herein, we show how the mixed-link approach could be used to make a series of new ZIFs based on the chabazite (**CHA**) zeolite topology.[7,8] Specifically, we report the synthesis and detailed characterization of an isoreticular series of ZIFs, in which 5(6)-bromobenzimidazolate (bbIm), 5(6)-chlorobenzimidazolate (cbIm), or 5(6)-methylbenzimidazolate (mbIm) was used with Zn^{II} atoms and 2-methylimidazolate (2-mIm) to construct **CHA**-type ZIFs termed ZIF-300, ZIF-301, and ZIF-302, respectively (Scheme 1). Our design strategy was built upon the use of bulky hydrophobic links to produce ZIFs that are water stable and are capable of capturing CO_2[9] under practical humid conditions. Consequently, we report the remarkable hydrophobic properties and CO_2 capture abilities for all members of this series. We further demonstrate that each member shows sufficient separation of CO_2 from a ternary mixture containing N_2 and water over three cycles. This occurred without degradation of the ZIF structure or performance.

ZIF-300, ZIF-301, and ZIF-302 were solvothermally synthesized using the mixture of 2-mImH and the respective benzimidazole derivative (Scheme 1). As a representative example, ZIF-300 was synthesized by dispensing 2-mImH, bbImH, and zinc nitrate tetrahydrate in a *N,N*-dimethylformamide (DMF) and water solvent mixture that was heated at 120 °C for 72 h to give light-brown block-shaped crystals (see Supporting Information). In contrast to other mixed-link ZIF syntheses,[5,6,10] water was used as a co-solvent and is believed to also play an important role in the formation of these ZIF compounds, especially of the **CHA** topology. This is supported by the fact that the **CHA** topology could not be obtained after exhaustive efforts were undertaken to form these frameworks in the absence of water. Prior to single-crystal X-ray diffraction analysis, the obtained crystalline materials were washed with DMF (5 × 3 mL) to remove all unreacted starting materials.

The crystal structures[11] of all members of this series show tetrahedral Zn atoms being surrounded by four Im links (Figure S1–S6 in the Supporting Information). These tetrahedral Zn atoms are then linked together by imidazolate

[*] N. T. T. Nguyen, Dr. H. T. Nguyen, K. E. Cordova
Center for Molecular and NanoArchitecture (MANAR)
Vietnam National University, Ho Chi Minh City (VNU - HCM)
Ho Chi Minh City, 721337 (Vietnam)
Dr. H. Furukawa, Dr. F. Gándara, K. E. Cordova, Prof. O. M. Yaghi
Department of Chemistry, University of California - Berkeley,
Materials Sciences Division, Lawrence Berkeley National Laboratory, Kavli Energy NanoSciences Institute at Berkeley, Center for Global Science at Berkeley
Berkeley, CA 94720 (USA)
E-mail: yaghi@berkeley.edu
Prof. O. M. Yaghi
King Fahd University of Petroleum and Minerals
Dhahran (Saudi Arabia)

[**] The work at MANAR was supported by the Ministry of Science and Technology (Vietnam) under grant number 38/2012/HĐ-NĐT. We thank Mr. T. B. Le, Mr. A. N. Tran, and Dr. A. T. L. Nguyen at MANAR for their valuable discussions and assistance. We also thank Mr. J. Jiang (UC Berkeley) for his assistance with NMR measurements. We acknowledge Drs. S. Teat and K. Gagnon (Advanced Light Source, ALS, Lawrence Berkeley National Laboratory) for support during the single-crystal diffraction data acquisition at the beam line 11.3.1. Work at the ALS was supported by the Office of Science, Office of Basic Energy Sciences, of the U.S. DOE under Contract No.DE-AC02-05CH11231.

Supporting information for this article is available on the WWW under http://dx.doi.org/10.1002/anie.201403980.

 © 2014 Wiley-VCH Verlag GmbH & Co. KGaA, Weinheim

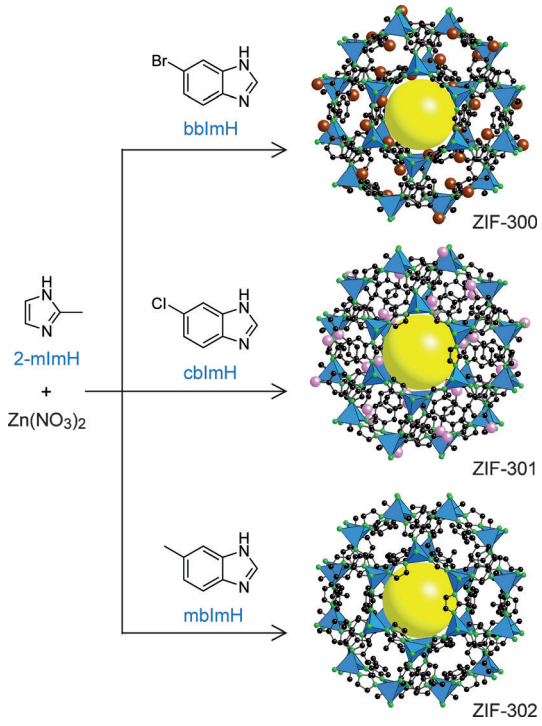

Scheme 1. Reaction of 2-methylimidazole (2-mImH) with $Zn(NO_3)_2$ and 5(6)-bromobenzimidazole (bbImH), 5(6)-chlorobenzimidazole (cbImH), or 5(6)-methylbenzimidazole (mbImH) resulting in ZIF-300, ZIF-301, and ZIF-302, respectively. The yellow sphere represents the space in the framework. Zn blue polyhedra, C black, N green, Br brown, Cl pink, all H atoms and terminal ligands are omitted for clarity.

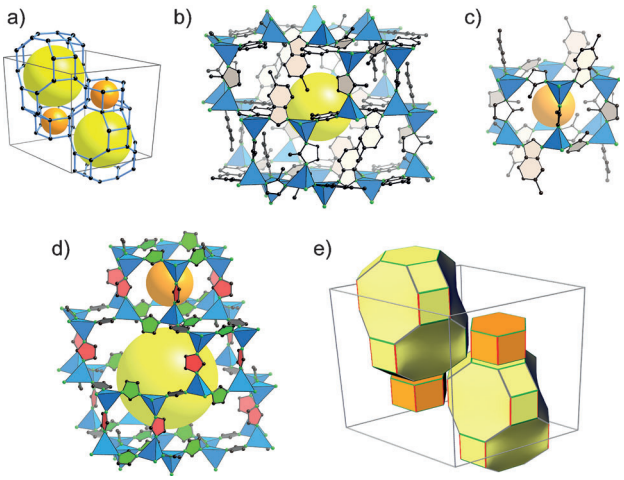

Figure 1. a) Ball-and-stick model depicting the **CHA** net. The yellow and orange spheres represent the space in the framework. b,c) The crystal structure of ZIF-302 is composed of two types of cages, *cha* (b) and *hpr* (c). d) These two types of cages, *cha* (large) and *hpr* (small) are cross-linked together. Light red and gray imidazolate rings indicate the specific position of 2-mIm and the corresponding bIm, respectively. The green imidazolate rings indicate the nonspecific positions, which 2-mIm or bIm can occupy. Functional groups are omitted for clarity. e) **CHA** tiling, with both the *cha* (yellow polyhedra) and *hpr* (orange polyhedra) cages, demonstrating which links occupy each of the unique edges (same color scheme as in (d). Zn blue polyhedra, C black. N green; all H atoms and terminal ligands are omitted for clarity.

bridges to produce the three-dimensional **CHA** framework (Figure 1 a). The **CHA**-type ZIF structure is illustrated by a *cha* $[4^{12}6^{2}8^{6}]$ cage (Figure 1 b), composed of 36 Zn tetrahedral vertices, cross-linked by a *hpr* $[4^{6}6^{2}]$ cage (Figure 1 c) with 12 such vertices in a ratio 1:1 (Figure 1 d,e) (the symbol $[..m^{n}..]$ means that there are n faces with m-membered rings).[12] This forms channels of 6-membered rings parallel to the c axis. The **CHA** topology includes four crystallographically distinct edges. Upon closer examination of the crystal structures, we found that in the case of all members, 2-mIm links (red in Figure 1 d,e) are always found at the edge that connects the two 6-membered rings comprising the *hpr* cage. Additionally, the substituted bIm links (gray in Figure 1 d,e) have specific positions within the *cha* cages, which are not edge sharing with the *hpr* cages. The remaining two edges (green in Figure 1 d,e), shared by the *hpr* and *cha* cages, are nonspecific with respect to either 2-mIm or the substituted bIm for ZIF-300 and ZIF-301. For ZIF-302, although it exhibits the same connectivity, mbIm was found to prominently occupy one of these two nonspecific edges. This situation is likely a result of a higher ratio of mbIm used in the synthesis to optimize the conditions for single-crystal growth.

The phase purity of ZIF-300 to ZIF-302 was demonstrated by the homogeneous crystal morphology observed in scanning electron microscope images (Figure S7–S9) as well as the noted good agreement between the experimental powder X-ray diffraction (PXRD) patterns with the PXRD patterns simulated from the single crystal structures (Figure S10–S12). To evaluate the structural characteristics of these ZIFs, the samples were solvent-exchanged and activated (see Supporting Information). Thermal gravimetric analysis on the activated samples demonstrated high thermal stability (450 °C) and confirmed the lack of guest molecules for all members (Figure S13–S15).

The crystallinity of these activated ZIFs was also confirmed by PXRD analysis (Figure S10–S12), which indicated the structural maintenance of all three members under such activation procedures. The permanent porosity of guest free samples was established by Ar gas-adsorption measurements at 87 K, which exhibited typical Type-I isotherms characteristic of microporous materials (Figure S16). The Langmuir (Brunauer–Emmet–Teller) surface areas were 490 (420), 825 (680), and 270 (240) $m^{2}g^{-1}$ for ZIF-300, ZIF-301, and ZIF-302, respectively.

As a result of the incorporation of hydrophobic functionalities within all three ZIFs, we sought to clearly demonstrate the materials' exceptional water stability. This was accomplished by soaking each ZIF structure in water at 100 °C for 7 days. Throughout this process, sample aliquots were taken for structural analysis by PXRD. The well-maintained diffraction patterns, as indicated by coincidence of peaks, signified that all three ZIFs were extremely stable in boiling water (Figure S17–S19). Following this lead, water adsorption measurements were performed (Figure S20). All ZIF members exhibited Type-III water isotherms, which are attributed to the hydrophobic functionalities throughout the frameworks.

© 2014 Wiley-VCH Verlag GmbH & Co. KGaA, Weinheim

Table 1: Chemical formula, surface area, crystal density, thermodynamic CO_2 uptake, CO_2/N_2 selectivity, dynamic CO_2 uptake for ZIF-300, ZIF-301, and ZIF-302.

ZIF-n	Chemical formula	A_{BET} $[m^2 g^{-1}]$[a]	Crystal density $[m^2 g^{-1}]$[b]	CO_2 uptake $[cm^3 cm^{-3}]$[c]	N_2 uptake $[cm^3 cm^{-3}]$[c]	CO_2/N_2 selectivity[d]	CO_2 uptake capacity-dry $[cm^3 cm^{-3}]$[e]	CO_2 uptake capacity-wet $[cm^3 cm^{-3}]$[e]
ZIF-300	$Zn(2\text{-mIm})_{0.86}(bbIm)_{1.14}\cdot(DMF)_{0.09}$	420	1.446	40	2.9	22	10.4	10.2
ZIF-301	$Zn(2\text{-mIm})_{0.94}(cbIm)_{1.06}\cdot(DMF)_{0.03}$	680	1.261	40	3.8	19	8.0	8.2
ZIF-302	$Zn(2\text{-mIm})_{0.67}(mbIm)_{1.33}\cdot(H_2O)_{0.5}$	240	1.193	36	4.0	17	5.5	5.6

[a] Calculated by BET method. [b] Calculated for activated ZIFs. [c] At 800 Torr and 298 K. [d] Calculated from pure component isotherms by Henry's law. [e] Calculated from dynamic breakthrough experiments.

For the industrially relevant process of post-combustion CO_2 capture from flue gas, adsorbents must be able to effectively separate CO_2 in the presence of nitrogen and other constituents, such as water.[13] Accordingly, the thermodynamic CO_2 and N_2 uptake of all three ZIFs were measured at 273, 283, and 298 K (Figure S21–S27). The isotherms for both CO_2 and N_2 at all measured temperatures exhibit a reversible adsorption and desorption process and there is clear indication that these ZIFs show higher capacity and affinity for CO_2 over N_2 (Figure S28). The CO_2 (N_2) capacities at 298 K and 800 Torr were 40 (2.9), 40 (3.8), and 36 (4.0) $cm^3 cm^{-3}$ for ZIF-300, ZIF-301, and ZIF-302, respectively. Furthermore, it is also noted that the initial slopes of the CO_2 isotherms were steeper than those observed for N_2, indicating the ZIFs higher affinity for CO_2. This led to the estimation of the CO_2/N_2 selectivity for each ZIF by calculating the ratios of the initial slopes based on Henry's law (Table 1, see Supporting Information).

Dynamic breakthrough experiments were performed to definitively show the CO_2 separation capabilities, as related to practical industrial processes, for all members of this series (Figure 2; Figure S29). In these experiments, an adsorbent material is exposed to a mixed gas stream to evaluate the time in which the material can selectively hold CO_2 while the other gas components pass through. A longer resulting CO_2 retention time (i.e. the time it takes for CO_2 to breakthrough) indicates a greater dynamic separation capacity. Accordingly, each ZIF sample was subjected to a flow of binary gas mixture comprising 16% (*v*/*v*) CO_2 and 84% (*v*/*v*) N_2, which simulated the appropriate volumetric percentages in flue gas streams. The resulting breakthrough curves clearly confirmed the fact that CO_2 was retained, while N_2 passed through unencumbered (Figure 2a). From these breakthrough measurements, the calculated CO_2 uptake capacities for ZIF-300, ZIF-301, and ZIF-302 were 10.4, 8.0, and 5.5 $cm^3 cm^{-3}$, respectively. It is worth noting that the capacity of dynamic CO_2 separation of these ZIFs increases with an increase in the calculated CO_2/N_2 selectivity (Figure S30).

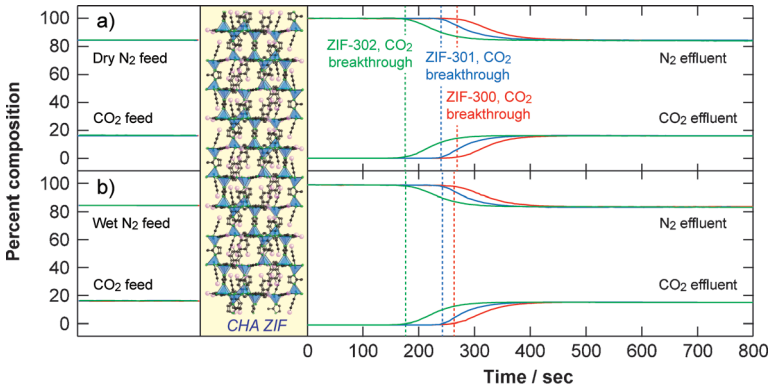

Figure 2. A binary mixture of CO_2 and dry N_2 (a) or wet (80% relative humidity) N_2 (b) is flown through a fixed bed of ZIF-300 (red), ZIF-301 (blue), and ZIF-302 (green). The breakthrough time is indicated by the dashed line.

Taking into consideration the water stability and hydrophobicity of ZIF-300, ZIF-301, and ZIF-302, we additionally sought to test these materials' ability to separate CO_2 from N_2 under humid conditions. This is an important factor to consider as similar materials have exhibited a noticeable decrease in CO_2 uptake capacity in the presence of water,[14] although there are a few exceptions to this otherwise.[15] Each ZIF structure was thus exposed to a wet N_2 gas stream (80% relative humidity) until water saturation was detected. Breakthrough experiments were then implemented by adding dry CO_2 to the binary gas mixture. As shown in Figure 2b, the breakthrough time was fully reproducible regardless of dry or humid conditions, which is evidence for the viability of these materials in carbon dioxide capture from flue gas (Table S4).

Low energy consumption and time efficiency throughout the regeneration and recycling process are of high importance in industrial settings.[16] For the case of each **CHA**-type ZIF, regeneration was fully realized under mild conditions. Specifically, the CO_2 saturated ZIF-300 was simply exposed to a N_2 pure flow at ambient temperature and within 15 min, 99.5% of adsorbed CO_2 was purged from the bed. For ZIF-301 and ZIF-302, the time needed for regeneration was less than 10 min. Remarkably, over the course of three cycling measurements, all three ZIF structures were shown to fully retain their CO_2 separation performance after successive regenerations (Figure S31–S36). Therefore, due to their performance under humid conditions coupled with their low energy regeneration requirements, these **CHA**-type ZIFs have overcome key challenges that many porous materials[14a–d,15b,c,17] face in rationalizing their use for practical applications.[13c]

© 2014 Wiley-VCH Verlag GmbH & Co. KGaA, Weinheim

Received: April 3, 2014
Revised: June 5, 2014
Published online: July 17, 2014

Keywords: carbon dioxide · dynamic separation · hydrophobic · metal–organic frameworks · zeolitic imidazolate frameworks

[1] a) K. S. Park, Z. Ni, A. P. Côté, J. Y. Choi, R. Huang, F. J. Uribe-Romo, H. K. Chae, M. O'Keeffe, O. M. Yaghi, *Proc. Natl. Acad. Sci. USA* **2006**, *103*, 10186 – 10191; b) X.-C. Huang, Y.-Y. Lin, J.-P. Zhang, X.-M. Chen, *Angew. Chem.* **2006**, *118*, 1587 – 1589; *Angew. Chem. Int. Ed.* **2006**, *45*, 1557 – 1559.

[2] A. Phan, C. J. Doonan, F. J. Uribe-Romo, C. Knobler, M. O'Keeffe, O. M. Yaghi, *Acc. Chem. Res.* **2009**, *42*, 58 – 67.

[3] H. Hayashi, A. P. Côté, H. Furukawa, M. O'Keeffe, O. M. Yaghi, *Nat. Mater.* **2007**, *6*, 501 – 506.

[4] C. Baerlocher, L. B. McCusker, D. H. Olson, *Atlas of Zeolite Framework Types 5th ed.*, Elsevier, Amsterdam, **2001**.

[5] R. Banerjee, A. Phan, B. Wang, C. Knobler, H. Furukawa, M. O'Keeffe, O. M. Yaghi, *Science* **2008**, *319*, 939 – 943.

[6] R. Banerjee, H. Furukawa, D. Britt, C. Knobler, M. O'Keeffe, O. M. Yaghi, *J. Am. Chem. Soc.* **2009**, *131*, 3875 – 3877.

[7] a) H. van Heyden, S. Mintova, T. Bein, *Chem. Mater.* **2008**, *20*, 2956 – 2963; b) J. Q. Chen, A. Bozzano, B. Glover, T. Fuglerud, S. Kvisle, *Catal. Today* **2005**, *106*, 103 – 107; c) U. Olsbye, S. Svelle, M. Bjørgen, P. Beato, T. V. W. Janssens, F. Joensen, S. Bordiga, K. P. Lillerud, *Angew. Chem.* **2012**, *124*, 5910 – 5933; *Angew. Chem. Int. Ed.* **2012**, *51*, 5810 – 5831.

[8] A structure equivalent to ZIF-301 has been reported. In that report, only the unit-cell parameters and the positions of the zinc ions were determined. Therefore, the atomistic connectivity, including link distribution and substituent positions, was not fully resolved and the exact structure of the **CHA**-type ZIF remained unknown up to our present report. D. Peralta, G. Chaplais, A. Simon-Masseron, K. Barthelet, G. D. Pirngruber, *Ind. Eng. Chem. Res.* **2012**, *51*, 4692 – 4702.

[9] a) S. Aguado, C.-H. Nicolas, V. Moizan-Baslé, C. Nieto, H. Amrouche, N. Bats, N. Audebrand, D. Farrusseng, *New J. Chem.* **2011**, *35*, 41 – 44; b) S. R. Venna, M. A. Carreon, *J. Am. Chem. Soc.* **2010**, *132*, 76 – 78; c) A. W. Thornton, D. Dubbeldam, M. S. Liu, B. P. Ladewig, A. J. Hill, M. R. Hill, *Energy Environ. Sci.* **2012**, *5*, 7637 – 7646.

[10] D. Peralta, G. Chaplais, A. Simon-Masseron, K. Barthelet, G. D. Pirngruber, *Microporous Mesoporous Mater.* **2012**, *153*, 1 – 7.

[11] Crystal structure refinement information: ZIF-300: trigonal, *R*-3, $a = 27.631(4)$, $c = 22.827(5)$ Å, $V = 15093.(5)$ Å^3, $T = 100$ K, $2\theta_{max} = 47.855°$, $M_r = 12280.85$, $Z = 1$, $\rho_{calcd} = 1.351$ g cm^{-3}, $Cu_{K\alpha} = 1.54178$ Å, $R_{int} = 0.0604$, R_1 $[I > 2\sigma(I)] = 0.1721$, wR_2 (all data) = 0.4953, 3017 independent reflections. ZIF-301: trigonal, *R*-3, $a = 27.590(6)$, $c = 21.891(4)$ Å, $V = 14431.(6)$ Å^3, $T = 100$ K, $2\theta_{max} = 27.106°$, $M_r = 10533.11$, $Z = 1$, $\rho_{calcd} = 1.2126$ g cm^{-3}, synchrotron radiation = 0.7749 Å, $R_{int} = 0.0813$, R_1 $[I > 2\sigma(I)] = 0.0883$, wR_2 (all data) = 0.2832, 5321 independent reflections. ZIF-302: trigonal, *R*-3, $a = 27.653(2)$, $c = 22.9284(19)$ Å, $V = 15184.(3)$ Å^3, $T = 100$ K, $2\theta_{max} = 44.57°$, $M_r = 10695.49$, $Z = 1$, $\rho_{calcd} = 1.170$ g cm^{-3}, $Cu_{K\alpha} = 1.54178$ Å, $R_{int} = 0.0879$, R_1 $[I > 2\sigma(I)] = 0.0828$, wR_2 (all data) = 0.2555, 2663 independent reflections. Further details are provided in the Supporting Information. Crystallographic data for ZIF-300, ZIF-301, and ZIF-302 were deposited in the Cambridge Crystallographic Data Center (CCDC). The deposition numbers are 995218, 995219, and 995220. This data can be obtained free of charge from The Cambridge Crystallographic Data Centre via www.ccdc.cam.ac.uk/data_request/cif.

[12] M. O'Keeffe, M. A. Peskov, S. J. Ramsden, O. M. Yaghi, *Acc. Chem. Res.* **2008**, *41*, 1782 – 1789.

[13] a) S. Keskin, T. M. van Heest, D. S. Sholl, *ChemSusChem* **2010**, *3*, 879 – 891; b) K. Sumida, D. L. Rogow, J. A. Mason, T. M. McDonald, E. D. Bloch, Z. R. Herm, T.-H. Bae, J. R. Long, *Chem. Rev.* **2012**, *112*, 724 – 781; c) J. Liu, P. K. Thallapally, B. P. McGrail, D. R. Brown, J. Liu, *Chem. Soc. Rev.* **2012**, *41*, 2308 – 2322.

[14] a) A. C. Kizzie, A. G. Wong-Foy, A. J. Matzger, *Langmuir* **2011**, *27*, 6368 – 6373; b) F. Brandani, D. M. Ruthven, *Ind. Eng. Chem. Res.* **2004**, *43*, 8339 – 8344; c) J. Liu, J. Tian, P. K. Thallapally, B. P. McGrail, *J. Phys. Chem. C* **2012**, *116*, 9575 – 9581; d) J. Liu, Y. Wang, A. I. Benin, P. Jakubczak, R. R. Willis, M. D. LeVan, *Langmuir* **2010**, *26*, 14301 – 14307; e) Y. Wang, Y. Zhou, C. Liu, L. Zhou, *Colloids Surf. A* **2008**, *322*, 14 – 18; f) Z. Liang, M. Marshall, A. L. Chaffee, *Energy Fuels* **2009**, *23*, 2785 – 2789; g) Z. Liang, M. Marshall, A. L. Chaffee, *Microporous Mesoporous Mater.* **2010**, *132*, 305 – 310.

[15] a) G.-P. Hao, W.-C. Li, D. Qian, G.-H. Wang, W.-P. Zhang, T. Zhang, A.-Q. Wang, F. Schüth, H.-J. Bongard, A.-H. Lu, *J. Am. Chem. Soc.* **2011**, *133*, 11378 – 11388; b) D. Li, H. Furukawa, H. Deng, C. Liu, O. M. Yaghi, D. S. Eisenberg, *Proc. Natl. Acad. Sci. USA* **2014**, *111*, 191 – 196; c) P. Nugent, Y. Belmabkhout, S. D. Burd, A. J. Cairns, R. Luebke, K. Forrest, T. Pham, S. Ma, B. Space, L. Wojtas, M. Eddaoudi, M. J. Zaworotko, *Nature* **2013**, *495*, 80 – 84.

[16] M. T. Ho, G. W. Allinson, D. E. Wiley, *Ind. Eng. Chem. Res.* **2008**, *47*, 4883 – 4890.

[17] a) M. L. Gray, Y. Soong, K. J. Champagne, J. Baltrus, R. W. Stevens, Jr., P. Toochinda, S. S. C. Chuang, *Sep. Purif. Technol.* **2004**, *35*, 31 – 36; b) P. J. E. Harlick, F. H. Tezel, *Microporous Mesoporous Mater.* **2004**, *76*, 71 – 79.

© 2014 Wiley-VCH Verlag GmbH & Co. KGaA, Weinheim